TECNICA ITALIANA-Italian Journal of Engineering Science
Vol. 61+1, No. 1, June, 2018, pp. 6-11
Journal homepage: http://iieta.org/Journals/TI-IJES

Magnetic refrigeration: A comparison between MnAs and FeRh based alloys in the room temperature range

Ciro Aprea[1], Adriana Greco[2*], Angelo Maiorino[1], Claudia Masselli[1]

[1] Department of Industrial Engineering, University of Salerno, Via Giovanni Paolo II 132, 84084, Fisciano (SA), Italy
[2] Department of Industrial Engineering, University of Naples Federico II, P.le Tecchio 80, 80125, Napoli, Italy

Corresponding Author Email: adriana.greco@unina.it

https://doi.org/10.18280/ti-ijes.620101

Received: 5 January 2018
Accepted: 3 March 2018

Keywords:
magnetocaloric effect, inverse magnetic materials, $MnFeP_{0.45}As_{0.55}$, $Fe_{49}Rh_{51}$

ABSTRACT

This paper describes a two-dimensional (2D) multiphysics model of a parallel plate regenerator made of magnetocaloric material. The regenerator operates as a refrigerant for a magnetic refrigerator operating at room temperature on the strength of an Active Magnetic Regenerator (AMR) cycle. The model is able to simulate the thermofluidodynamic behavior of the magnetocaloric material and the magnetocaloric effect of the refrigerant. With this model direct ($MnFeP_{0.45}As_{0.55}$) and inverse ($Fe_{49}Rh_{51}$) magnetocaloric materials have been investigated. The tests were performed with fixed AMR cycle frequency (1.25 Hz), cold heat exchanger temperature (310 K), hot heat exchanger temperature (318 K), while secondary fluid flow rate was varied in the range 0.034÷0.057 kg/s. The secondary fluid used for simulations is liquid water. The results, generated for a magnetic induction which varies from 0 to 1.5 T, are presented in terms of temperature span, refrigeration power and coefficient of performance. Results clearly show that the best material from an efficiency's point of view is $Fe_{49}Rh_{51}$ which exhibits the highest values of ΔT_{span}, Q_{ref} and COP. Instead $MnFeP_{0.45}As_{0.55}$ shows, in this temperature range (centered around its Curie point), values of ΔT_{span}, Qref and COP too low for any kind of practical application.

1. INTRODUCTION

Magnetic refrigeration is an innovative, promising and ecologic technology, which aims to substitute the conventional vapor-compression refrigeration by the employment of solid materials as refrigerants instead of the fluid [1-5]. It is based on the Magneto-Caloric Effect (MCE), a physical phenomenon, related to solid-state materials with magnetic properties [6]. MCE consists in a coupling between the entropy of the Magnetocaloric Material (MM) and the variation of an external magnetic field applied to the material, which causes magnetic ordering in the MM structure. MCE is largest in the immediate vicinity of magnetic transition temperatures (Curie point). The two possible magnetic phase changes that one can observe at the Curie point are first order magnetic transition (FOMT) and second order magnetic transition (SOMT). At the Curie point a magnetic transition has FOMT characteristics when the material exhibits a discontinuity in the first derivative of the Gibbs free energy (G.f.e.), magnetization function, whereas has a SOMT behavior when the gap is detected in the second derivative of G.f.e., magnetic susceptibility, while its first derivative is a continuous function. Most of the magnetic materials order with a SOMT from a paramagnet to a ferromagnet, ferrimagnet or antiferromagnet. MCE can be referred to two different transformations, adiabatic or isothermal. If the magnetization is done isothermally, it will lower the material's magnetic entropy by the isothermal entropy change (ΔS_M). However, if the magnetization is done adiabatically, with no thermal transfer to the ambient, the total sample entropy remains constant and the decrease in magnetic entropy is countered by an increase in the lattice and electron entropy. This causes a heating of the material and a temperature increase given by the adiabatic temperature change (ΔT_{ad}). The inverse procedure also applies: under adiabatic demagnetization the magnetic entropy increases, causing a decrease in lattice vibrations and by that a temperature decrease. At its Curie temperature, where is located its own magnetic phase transition, a MM shows the peak of MCE, in terms of ΔT_{ad} and ΔS_M.

MCE can also be inverse. As opposed to cooling by adiabatic demagnetization, cooling by adiabatic magnetization (inverse MCE) requires an increase of configurational entropy on applying a magnetic field. The inverse MCE is observed in systems where first-order magnetic transformations, such as antiferromagnetic/ferromagnetic or antiferromagnetic /ferrimagnetic, takes place.

In this paper a comparison between a magnetic material with a direct and with an inverse MCE has been carried out.

In the family of magnetic materials with a direct MCE in the room temperature range there are MnAs alloys. Indeed, those compounds have a giant MCE exhibiting a first order magnetic transition; by varying alloy's composition, the Curie temperature could be switched in the range 220÷318 K. Anyway, MnAs shows also a thermal hysteresis that is bad for practical application. Among Mn-based compounds, $MnFeP_{1-x}As_x$ compounds that are stable for $0.15 < x < 0.66$ and exhibit interesting magnetic properties associated with a first order metamagnetic transition. The Curie temperature of the alloy increases linearly with the as contents. In the present paper compound $MnFeP_{0.45}As_{0.55}$, previously introduced by de Oliveira et al. [7], has been investigated; it undergoes a FOMT

from paramagnetic to ferromagnetic at 307 K (on heating) according to a rapid decrease of the material parameters which changes its Debye temperature and its electronic structure. The first order transition occurs at 302.8 K on cooling, and at 306.6 K on heating. This indicates a thermal hysteresis of 3.8 K. The change in volume at the transition temperature is about 2.2 %. The adiabatic temperature change for these compounds is relatively low and the thermal conductivity is significantly lower than that of gadolinium and other magnetic materials.

In the family of the inverse magnetocaloric materials there are Fe-Rh compounds [8]. These compounds show a field induced antiferromagnetic-ferromagnetic first order magnetic phase transition. In particular, we have considered the compound $Fe_{49}Rh_{51}$ that shows the transition at 313K with a thermal hysteresis around 8.5 K.

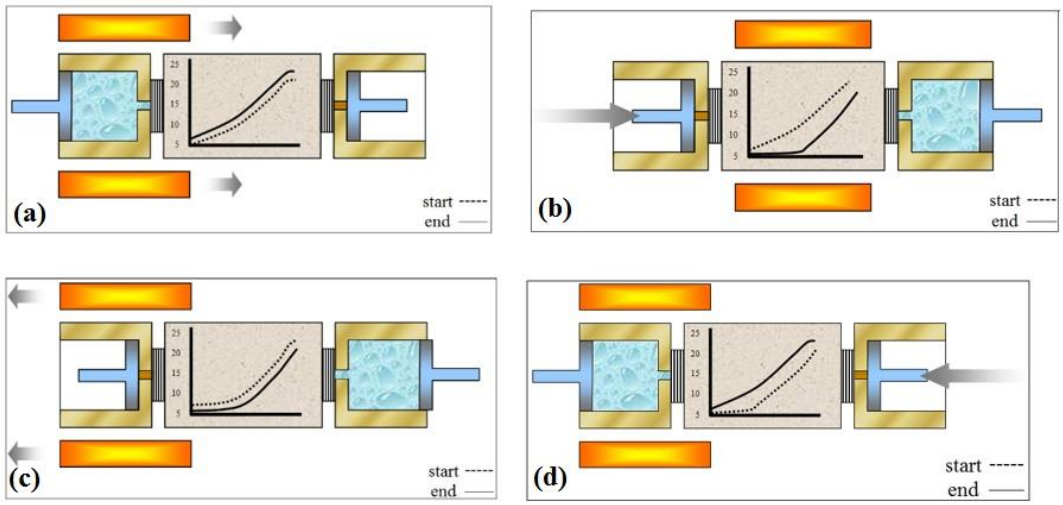

Figure 1. The AMR cycle for a direct magnetic material

A magnetic refrigeration cycle, based on the MCE, consists of magnetization and demagnetization of a magnetic material in which heat is expelled and absorbed respectively, and two other benign middle processes. In an Active Magnetic Regenerative refrigeration cycle (AMR) two separate processes are coupled into a single one. Instead of using a separate material as a regenerator to recuperate the heat from the magnetic material, the AMR concept made use the magnetic material as a refrigerant and as a regenerator. An active magnetic regenerator can provide larger temperature spans with adequate heat transfer between the regenerator matrix and a heat transfer fluid. The working principle of an AMR is presented in Figure 1. For instance, let's assume that the bed is at a steady state condition with the hot heat exchanger at Th and the cold heat exchanger at Tc. Four processes are present in the AMR cycle: (a) adiabatic magnetization: each particle in the bed warms up; (b) isofield cooling: the high field is present, the fluid is blown from the cold end to the hot end, and it absorbs heat from the bed and expels heat at a temperature higher that Th in the hot heat exchanger; (c) adiabatic demagnetization: each particle in the bed cools again; (d) isofield heating: the field is zero, the fluid is blown from the hot end to the cold end, and it expels heat to the particles of the bed and absorbs heat at a temperature lower than Tc in the cold heat exchanger. In Figure 1 the dashed line represents the initial temperature profile of the bed in each process while the solid line represents the final temperature profile of that process. If the material has an indirect effect the process of magnetization and demagnetization can be exchanged, and therefore the processes are: (a) adiabatic demagnetization: each particle in the bed warms up; (b) isofield cooling: at zero field the fluid is blown from the cold end to the hot end, and it absorbs heat from the bed and expels heat in the hot heat exchanger; (c) adiabatic magnetization: each particle in the bed cools; (d) isofield heating: the field is maximum, the fluid is blown from the hot end to the cold end, and it expels heat to the particles of the bed and absorbs heat in the cold heat exchanger.

The main goal of this paper is to make a comparison between $MnFeP_{0.45}As_{0.55}$ and $Fe_{49}Rh_{51}$ working in an AMR cycle in the room temperature range. To this hope, a practical 2D model for predicting the refrigeration capacity and the efficiency of an AMR cycle has been developed.

2. DESCRIPTION OF THE 2D MODEL

The model presented in this paper is of a two-dimensional porous regenerator operating at room temperature. The regenerator has a rectangular shape with a height of 20mm and a length of 45 mm. The area of the regenerator is filled with a regular matrix of 3600 circles that constitute the porous media; every circle has a diameter of 0.45mm and the amount of the area occupied by all of the circles is 63% of the total rectangular area. A group of channels is formed by stacking particles in the regenerator area: the fluid flows through these interstitial channels. The regenerator's geometry has been chosen according to the characteristics of one of the eight regenerators of the experimental prototype developed at the Refrigeration Lab in the University of Salerno in collaboration with the University of Naples Federico II [9-13]. In this model both the fluid flow and heat transfer between the solid and the fluid have been taken in account. The fluid flows in the positive x direction during the isofield cooling process and in the opposite direction during isofield heating [14-22].

The equations that rule the regenerative fluid flow processes, in both directions, are: the Navier-Stokes equations for the fluid flow and the energy equations for both the fluid and the solid particles. With the assumptions that the fluid is incompressible, the viscous dissipation in neglected, due to

low mass flow, the above equations are as follows:

$$\begin{cases} \dfrac{\partial u}{\partial x}+\dfrac{\partial v}{\partial y}=0 \\ \dfrac{\partial u}{\partial t}+u\dfrac{\partial u}{\partial x}+v\dfrac{\partial u}{\partial y}=-\dfrac{1}{\rho_f}\dfrac{\partial p}{\partial x}+\upsilon\left(\dfrac{\partial^2 u}{\partial x^2}+\dfrac{\partial^2 u}{\partial y^2}\right) \\ \dfrac{\partial v}{\partial t}+u\dfrac{\partial v}{\partial x}+v\dfrac{\partial v}{\partial y}=-\dfrac{1}{\rho_f}\dfrac{\partial p}{\partial y}+\upsilon\left(\dfrac{\partial^2 v}{\partial x^2}+\dfrac{\partial^2 v}{\partial y^2}\right) \\ \dfrac{\partial T_f}{\partial t}+u\dfrac{\partial T_f}{\partial x}+v\dfrac{\partial T_f}{\partial y}=\dfrac{k_f}{\rho_f C_{fp}}\left(\dfrac{\partial^2 T_f}{\partial x^2}+\dfrac{\partial^2 T_f}{\partial y^2}\right) \\ \dfrac{\partial T_S}{\partial t}=\dfrac{k_S}{\rho_S C_{sp}}\left(\dfrac{\partial^2 T_S}{\partial x^2}+\dfrac{\partial^2 T_S}{\partial y^2}\right) \end{cases} \quad (1)$$

The equations that model the magnetization and the demagnetization process of the cycle must take into account the MCE which elevates or lowers the temperature of the solid by the variation of the external magnetic field applied to the regenerator. Hence the MCE temperature variation ΔT_{ad} is converted into a heat source Q*:

$$Q^* = Q^*(H,T_S) = \frac{\rho_S C_{sp}(H,T_S)\Delta T_{ad}(H,T_S)}{\Delta t} \quad (2)$$

which has the dimensions of a power density $[W/m^3]$ and included in the solid energy equation, only for magnetization and demagnetizations phases, as follows:

$$\rho_s C_{sp}\frac{\partial T_S}{\partial t}=k_s\left(\frac{\partial^2 T_S}{\partial x^2}+\frac{\partial^2 T_S}{\partial y^2}\right)+Q^* \quad (3)$$

The term Q* is positive during magnetization, negative during demagnetization for materials with direct magnetocaloric effect, the opposite for materials with inverse effect. Therefore, the equations that govern the magnetization and the demagnetization phases are:

$$\begin{cases} \rho_f C_{fp}\dfrac{\partial T_f}{\partial t}=k_f\left(\dfrac{\partial^2 T_f}{\partial x^2}+\dfrac{\partial^2 T_f}{\partial y^2}\right) \\ \rho_s C_{sp}\dfrac{\partial T_S}{\partial t}=k_s\left(\dfrac{\partial^2 T_S}{\partial x^2}+\dfrac{\partial^2 T_S}{\partial y^2}\right)+Q^* \end{cases} \quad (4)$$

The magnetic properties of the magnetocaloric materials have been evaluated interpolating experimental data available from the literature. The intensity of the magnetic field varies from 0 to the maximum value of 1.5 T during magnetization and from 1.5 T to 0 during demagnetization.

Figure 2 reports Q*Δt as a function of temperature in the magnetization process, where Δt is the period of the magnetization/demagnetization process for $Fe_{49}Rh_{51}$. Circles represent experimental data, whereas the continuous line is the curve fitting. In this figure it is possible to appreciate a minimum around the Curie temperature of the compound (313 K), where the inverse magnetocaloric effect is minimum.

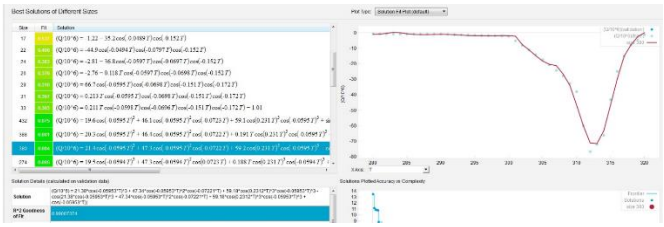

Figure 2. $Q^* * \Delta t$ as a function of temperature for $Fe_{49}Rh_{51}$ during magnetization from 0 to 1.5T

From the construction of a table function, who describes Q* in a range of temperature and magnetic field intensity, and by the help of a mathematical function finder software (Eureka Formulize), a mathematical expression for Q* has been found both for magnetization and demagnetization processes. In the follow equation is reported the expression found for $Fe_{49}Rh_{51}$:

$$Q*\Delta t = 10^6[21.4*\cos(-0.0595*T)^3+47.3*\cos(-0.0595*T)^2*\cos(-0.0722*T)+59.2*\cos(0.231*T)^3*\cos(-0.0595*T)^3-\cos(21.4*\cos(-0.0595*T)^3+47.34*\cos(-0.0595*T)^2)\cos(-0.0722*T)+59.2*\cos(0.231*T)^3*\cos(-0.0595*T)^3+\cos(-0.0595*T)] \quad (5)$$

Figure 3 reports Q*Δt as a function of temperature in the magnetization process for $MnFeP_{0.45}As_{0.55}$. In this figure it is possible to appreciate a maximum around the Curie temperature of the compound (315 K), where the direct magnetocaloric effect is maximum.

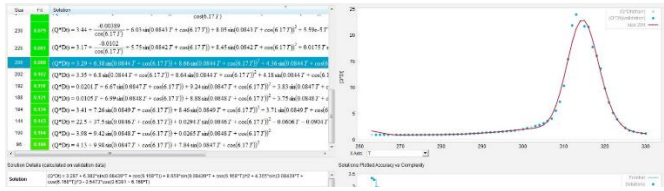

Figure 3. $Q^* * \Delta t$ as a function of temperature for $MnFeP_{0.45}As_{0.55}$ during magnetization from 0 to 1.5T

Interpolating the experimental data, the following expression has been found for $MnFeP_{0.45}As_{0.55}$:

$$Q^*\Delta t = 10^6[3.29+6.38*\sin(0.0844*T+\cos(6.17*T))+8.66\sin(0.0844*T+\cos(6.17*T))^2+4.36*\sin(0.0844*T+\cos(6.17*T))^3-0.547*\cos(0.639+6.17*T)] \quad (6)$$

In the following, the boundary conditions for each process are described in detail:

- magnetization/demagnetization: during the magnetization and demagnetization processes, the fluid is stationary; thus, thermal insulation is applied on all the regenerator walls;
- fluid flow processes from/toward hot heat exchanger: the boundary condition for modeling fluid velocity and direction requires the construction of a velocity vector **u** that is positive during the fluid flow processes toward the hot heat exchanger and negative otherwise. The presence of the hot heat exchanger during the fluid flow process is modeled by the imposition of its temperature on the right boundary of the regenerator.

The coupled equations that govern the AMR cycle, imposed on this model, are solved using Finite Element Method. The AMR cycle is modelled as four sequential steps. The initial condition of every step is the final condition of the preceding one, so that time-based sequential condition is applied. The same time step Δt has been chosen for the resolution during all the four periods of the cycle. The cycle has been repeated several times with constant frequency until the regenerator reaches steady state operation.

The refrigeration energy and the energy supplied in the environment are calculated according to the following

equations:

$$Q_{rej} = \int_{3\Delta t}^{4\Delta t} \dot{m}_f C_f \left(T_c - T_f(0,y,t)\right) dt \quad (7)$$

$$Q_{rej} = \int_{\Delta t}^{2\Delta t} \dot{m}_f C_f \left(T_f(L,y,t) - T_H\right) dt \quad (8)$$

The Coefficient of Performance is evaluated as:

$$COP = \frac{Q_{ref}}{Q_{rej} - Q_{ref} + W_p} \quad (9)$$

ΔT_{span} has also been obtained evaluating the difference between T_H and the cold side temperature of the regenerator averaged in the last process of AMR cycle (fluid flow from hot to cold side of the regenerator), as show in the equation:

$$\Delta T_{span} = T_H - \int_{3\Delta t}^{4\Delta t} T_f(0,y,t)\, dt \quad (10)$$

3. RESULTS

By means of the simulation with the previous equations, integrated with the boundary and the initial conditions, the refrigeration power, COP, the temperature profile of the magnetic bed and of the regenerating fluid have been obtained. In the simulations the temperature range that has been explored is 310 – 318 K. The secondary fluid used in this temperature range is liquid water. Indeed, in this temperature range water is the best secondary fluid because has low viscosity (therefore needs a low work of the pump) and high values of specific heat and of thermal conductivity. The fluid flow rate was varied in the range 0.034÷0.057 kg/s.

Figure 4 shows the design of the regenerator: a white stack of plates bounded by a H x L packaging (20 x 45 mm^2) forms the caloric solid-state refrigerant; whereas in yellow are the channels for fluid crossing. Each solid-state plate is 0.25mm thick; the distance between two plates is 0.125 mm and it corresponds to the thickness of a single channel. Dually the distance between two channels is 0.25 mm.

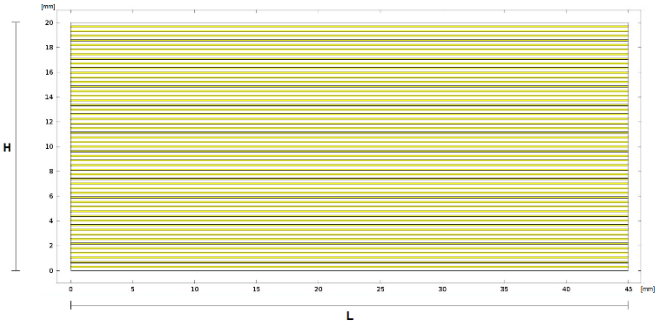

Figure 4. Design of the magnetocaloric model

The aim of this work is to make a comparison between inverse ($Fe_{49}Rh_{51}$) and direct ($MnFeP_{0.45}As_{0.55}$) magnetic material working in the same operating conditions.

In figure 5 one can see ΔT_{span} as a function of fluid flow rate.

The general trend shows that the temperature span slightly decreases with the water mass flow rate. Indeed, corresponding to a small fluid mass flow rate, the fluid can be regenerated to reach lower cold side temperature. Figure 5 clearly shows that the most performant material is the inverse magnetic material $Fe_{49}Rh_{51}$. In particular, the latter shows a ΔT_{span} always higher than 12 K, whereas $MnFeP_{0.45}As_{0.55}$ shows a ΔT_{span} around 8 K.

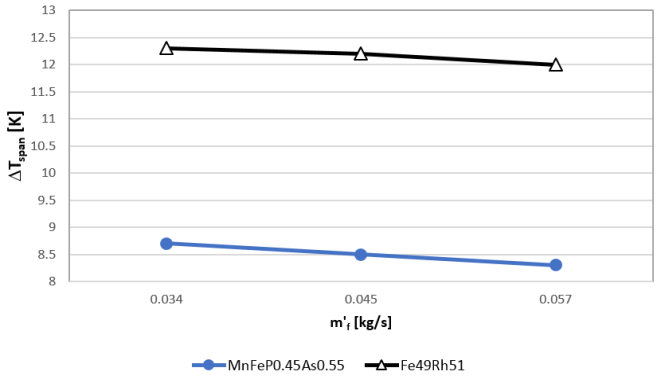

Figure 5. ΔT_{span} vs $\dot{m}_f$ for ferromagnetic and anti-ferromagnetic solid-state refrigerants

In Figure 6 is shown the refrigerating power as a function of water flow rate for both the materials. An increase of the water mass flow rate increases the refrigerating power. Indeed, refrigerating power has a direct proportionality with the fluid mass flow rate. The Figure clearly shows that the refrigerant power pertaining to $Fe_{49}Rh_{51}$ is always greater than that of $MnFeP_{0.45}As_{0.55}$ (with a mean value of +90%). While the cooling power of $Fe_{49}Rh_{51}$ can be used for small-scale refrigerators, instead, that pertaining to $MnFeP_{0.45}As_{0.55}$ is too low for any kind of practical application.

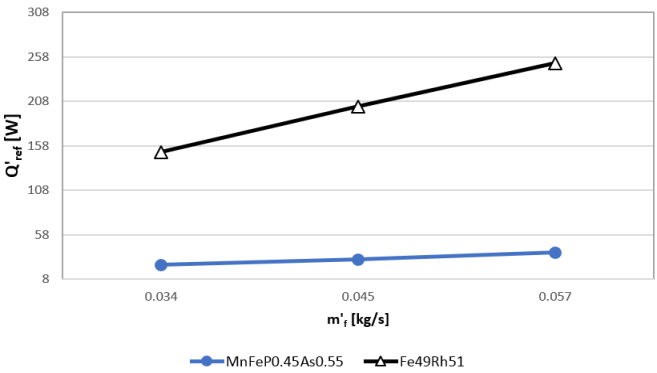

Figure 6. $\dot{Q}_{ref}$ vs $\dot{m}_f$ for ferromagnetic and anti-ferromagnetic solid-state refrigerants

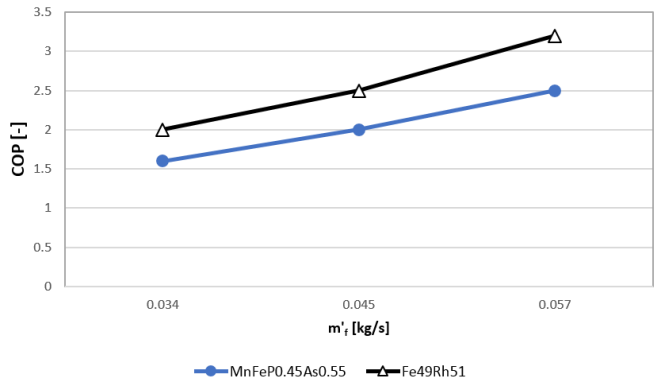

Figure 7. COP vs $\dot{m}_f$ for ferromagnetic and anti-ferromagnetic solid-state refrigerants

Figure 7 illustrates the Coefficient of Performance (COP) evaluated for both the materials presented in this work. As the refrigerant power, COP increases according to the increase of the water flow rate too.

Figure 7 clearly shows that the COP of $Fe_{49}Rh_{51}$ is always better than that of $MnFeP_{0.45}As_{0.55}$ (from a minimum of +10 % to a maximum of +21%).

4. CONCLUSIONS

Direct ($MnFeP_{0.45}As_{0.55}$) and inverse ($Fe_{49}Rh_{51}$) magnetocaloric materials have been investigated through a 2D numerical model of a parallel plates active magnetic regenerator. This model accounts for the coupled effects of temperature and velocity fields. The tests were performed with fixed AMR cycle frequency (1.25 Hz), cold heat exchanger temperature (310 K), hot heat exchanger temperature (318 K), while secondary fluid flow rate was varied in the range 0.034÷0.057 kg/s. The secondary fluid used for simulations is liquid water. The results, generated for a magnetic induction which varies from 0 to 1.5 T, are presented in terms of temperature span, refrigeration power and coefficient of performance. Results clearly show that the best material from an efficiency's point of view is $Fe_{49}Rh_{51}$ which exhibits the highest values of ΔT_{span}, Q_{ref} and COP. Instead manganites show, in this temperature range (centred around its Curie point), values of ΔT_{span}, Q_{ref} and COP too low for any kind of practical application.

REFERENCES

[1] Gschneidner KA Jr, Pecharsky VK. (2008). Thirty years of near room temperature magnetic cooling: where we are today and future prospects. Int. Journal of Refrigeration 31(6): 945-961. https://doi.org/10.1016/j.ijrefrig.2008.01.004

[2] Theil Kuhn L, Pryds N, Bahl CRH, Smith A. (2011). Magnetic refrigeration at room temperature – from magnetocaloric materials to a prototype. Journal of Physics: Conference Series 303(1) https://doi.org/10.1088/1742-6596/303/1/012082

[3] Engelbrecth K, Pryds N. (2014). Progress in magnetic refrigeration and future challenges. 6th IIF-IIR Int. Conf. On Magnetic Refrigeration, Victoria, BC, pp. 7-10.

[4] Aprea C, Greco A, Maiorino A. (2016). Magnetic refrigeration: a promising new technology for energy saving. International Journal of Ambient Energy 37(3): 294-313. https://doi.org/10.1088/1742-6596/655/1/012026

[5] Silva DJ, Bordalo BD, Pereira AM, Ventura J, Araújo JP. (2012). Solid state magnetic refrigerator. Applied Energy 93: 570-574. https://doi.org/10.1016/j.apenergy.2011.12.002

[6] Pecharsky VK, Gschneidner KA Jr. (2006). Advanced magnetocaloric materials: What does the future hold? Int. Journ. of Refrig. 29: 1239-1249. https://doi.org/10.1016/j.ijrefrig.2006.03.020

[7] de Oliveira NA, von Ranke PJ. (2005). Theoretical calculations of the magnetocaloric effect in $MnFeP_{0.45}As_{0.55}$ a model of itinerant electrons. Journal of Physics: Condensed Matter 17: 3325–3332.

[8] Annaorazov MP, Asatryan KA, Myalikgulyev G, Nikitin SA, Tishin AM, Tyurin AL. (1992). Alloys of the Fe-Rh system as a new class of working material for magnetic refrigerators. Cryogenics 32(10): 867-872. https://doi.org/10.1016/0011-2275(92)90352-B

[9] Aprea C, Greco A, Maiorino A, Mastrullo R, Tura A. (2014). Initial experimental results from a rotary permanent magnet magnetic refrigerator. International Journal of Refrigeration 43: 111-122. https://doi.org/10.1016/j.ijrefrig.2014.03.014

[10] Aprea C, Greco A, Maiorino A. (2015). GeoThermag: a geothermal magnetic refrigerator. International Journal of Refrigeration 59: 75-83. https://doi.org/10.1016/j.ijrefrig.2015.07.014

[11] Aprea C, Greco A, Maiorino A, Masselli C. (2016). The energy performances of a rotary permanent magnet magnetic refrigerator. International Journal of Refrigeration 61: 1-11. https://doi.org/10.1016/j.ijrefrig.2015.09.005

[12] Aprea C, Cardillo G, Greco A, Maiorino A, Masselli C. (2016). A rotary permanent magnet magnetic refrigerator based on AMR cycle. Applied Thermal Engineering 101: 699-703. https://doi.org/10.1016/j.applthermaleng.2016.01.097

[13] Aprea C, Greco A, Maiorino A. (2017). An application of the artificial neural network to optimise the energy performances of a magnetic refrigerator. International Journal of Refrigeration 82: 238-251. https://doi.org/10.1016/j.ijrefrig.2017.06.015

[14] Aprea C, Greco A, Maiorino A. (2011). A numerical analysis of an Active Magnetic Regenerative Cascade system. International Journal of Energy Research 35: 177-188. https://doi.org/10.1002/er.1682

[15] Aprea C, Greco A, Maiorino A. (2011). A numerical analysis of an Active Magnetic Regenerative Refrigerant system with a multi-layer regenerator. Energy Conversion and Management 52: 97-107. https://doi.org/10.1016/j.enconman.2010.06.048

[16] Aprea C, Greco A, Maiorino A. (2012). Modelling an Active Magnetic Refrigeration system: a comparison with different models of incompressible flow through a packed bed. Applied Thermal Engineering 36: 296-306. https://doi.org/10.1016/j.applthermaleng.2011.10.034

[17] Aprea C, Greco A, Maiorino A. (2013). The use of the first and of the second order phase magnetic transition alloys for an AMR refrigerator at room temperature: a numerical analysis of the energy performances. Energy Conversion and Management 70: 40-55. https://doi.org/10.1016/j.enconman.2013.02.006

[18] Aprea C, Greco A, Maiorino A. (2013). A dimensionless numerical analysis for the optimization of an AMR cycle. International Journal of Energy Research 37(12): 1475-1487. https://doi.org/10.1002/er.2955

[19] Aprea C, Greco A, Maiorino A, Masselli C. (2015). A comparison between experimental and 2D numerical results of a packed-bed active magnetic Regenerator. Applied Thermal Engineering 90: 376-383. https://doi.org/10.1016/j.applthermaleng.2015.07.020

[20] Aprea C, Greco A, Maiorino A, Masselli C. (2015). A comparison between rare earth and transition metals working as magnetic materials in an AMR refrigerator in the room temperature range. Appl. Thermal Eng. 91: 767-777. https://doi.org/10.1016/j.applthermaleng.2015.08.083

[21] Aprea C, Greco A, Maiorino A, Masselli C. (2015).

Magnetic refrigeration: an eco-friendly technology for the refrigeration at room temperature. Journal of Physics: Conference Series 655. https://doi.org/10.1088/1742-6596/655/1/012026

[22] Aprea C, Greco A, Maiorino A, Masselli C. (2017). Analyzing the energetic performances of AMR regenerator working with different magnetocaloric materials: investigations and viewpoints. International Journal of Heat and Technology 35(Special Issue 1): S383-S390. https://doi.org/10.18280/ijht.35Sp0152

NOMENCLATURE

B	magnetic field induction, T
C	specific heat, J. kg^{-1}. K^{-1}
H	magnetic field, A. m^{-1}
k	thermal conductivity, W.m^{-1}. K^{-1}
M	magnetization, A. m^{-1}
Q	energy, J
Q*	power density, W. m^{-3}
p	pressure, Pa
s	entropy, J. kg^{-1}. K^{-1}
T	temperature, K
t	time, s
u	longitudinal fluid velocity, m.s^{-1}
v	orthogonal fluid velocity, m.s^{-1}
W	work, J

Greek symbols

Δ	finite difference
μ	dynamic viscosity, kg. m^{-1}. s^{-1}
ν	cinematic viscosity, m^{+2}. s^{-1}
ρ	density, kg. m^{-3}
τ	time period of the cycle, s

Subscripts

0	minimum
1	maximum
ad	Adiabatic
C	cold heat exchanger
f	fluid
H	hot heat exchanger
P	constant pressure
ref	refrigerant
rej	rejected
s	solid